A microscopic view of chemically activated amorphous carbon nanofibers prepared from core/sheath melt-spinning of phenol formaldehyde-based polymer blends

Kuo-Kuang Cheng · Tzu-Chien Hsu ·
Li-Heng Kao

Abstract Based on a novel solvent-free coextrusion and melt-spinning of polypropylene/(phenol formaldehyde-polyethylene)-based core/sheath polymer blends, a series of activated carbon nanofibers (ACNFs) have been prepared and their morphological and microstructure characteristics analyzed by scanning electron microscopy, atomic force microscopy (AFM), Raman spectroscopy, and X-ray diffractometry with particular emphasis on the qualitative and quantitative AFM analysis. The effect of activating agent, potassium hydroxide, and phosphorous acid is compared, and factors affecting the surface morphology and microstructure of ACNF are analyzed.

Introduction

There are two processes for manufacturing the carbon nanofiber (CNF), namely, the vapor-grown approach and the polymer spinning approach. The vapor-grown approach is a relatively simple but expensive one which proceeds via laser vaporization, arc discharge, or chemical vapor deposition. The electro-spinning and polymer blend method is a well-known polymer spinning technique which incorporates polymer with solvent to produce sub-micron polymeric fibers. The activated carbon nanofiber (ACNF) is the

K.-K. Cheng · T.-C. Hsu (✉)
Department of Materials and Optoelectronic Science,
National Sun Yat-Sen University, Kaohsiung 80424, Taiwan
e-mail: tjhsu@facmail.nsysu.edu.tw
URL: http://www.mse.nsysu.edu.tw/people/bio.php?PID=8

L.-H. Kao
Department of Chemical and Materials Engineering,
National Kaohsiung University of Applied Science,
Kaohsiung 80778, Taiwan

physically or chemically activated CNF, which have been, in many investigations, practically applied in electric double layer capacitors [1–6], organic vapor recovery, catalyst support, hydrogen storage [7–11], and so on.

In practice, the physical activation method involves carbonizing the carbon precursors at high temperatures (>750 °C) and then activating CNF in an oxidizing atmosphere such as carbon dioxide or steam [7, 12–15]. The chemical activation method involves chemically activating agents such as alkali, alkaline earth metals, some bases such as potassium hydroxide (KOH) [1–9, 15–17] and sodium hydroxide [8, 11, 15, 17, 18], zinc chloride [17], and phosphoric acid (H_3PO_4) [14, 17, 19]. In essence, most chemical activation on CNF used KOH to get highly porous structure and higher specific surface area.

Normally, the vapor-grown CNF possess a relatively high crystallinity and, because of that, the porosity development during the activation process is quite restricted. On the other hand, the porosity development during the activation process is relatively easy for the electro-spun CNF due to their relative low crystallinity. Unfortunately, large amount of solvent were needed to prepare the polymer solution for electro-spinning and polymer blend, causing serious environmental problem thereafter.

A series of porous amorphous ACNF were studied by Oya et al. utilizing the core/shell microspheres which were made of various polymer blends with solvent. In their approach, the phenol formaldehyde-derived CNF were chemically activated by the alkaline hydroxides, and the thus-prepared ACNF were applied as super-capacitor electrodes and hydrogen storage materials [2, 8, 20]. This chemical activation method has been reported to lead to new micropores and larger surface areas, as well as a higher content of basic oxygen groups; all these contributed to a specific BET surface area (S_{BET}) of 1520 m^2/g

does and enhanced values of capacitance as high as 255, 202, and 87 F/g for the acidic, basic, and organic electrolytes, respectively. On the other hand, a total H_2 storage capacity around 34 g/L was reported for ACNF with a S_{BET} of only 1500–1700 m^2/g at 77 K and 40 bar, due mainly to the amorphous nature of the ACNF prepared. However, it should be noted that solvents such as acetone and toluene were required in the CNF precursor preparation process.

There have been several studies on the surface characterization of carbon nanotubes and CNFs using scanning and transmission electron microscopy, and scanning probe microscopy [14, 21–26], but seldom by atomic force microscopy (AFM), as far as the surface morphology or topology is concerned. Figueiredo et al. reported a nano-scaled surface topography of vapor-grown and air or carbon dioxide-activated carbon fibers by AFM [27]. Work by Bellucci et al. adopted the AFM to realize a 3D nanoscale topography and morphology profile of the micro and nanoscaled carbon nanotubes [28]. To the best of our knowledge, there has been no report on surface morphology associated with chemical activation conditions of CNF at nanometer scale, not to mention the quantitative description, by AFM.

We have reported, based on a polymeric raw material system of polypropylene/(phenol formaldehyde/polyethylene) [PP/(PF/PE)], a novel approach for making CNF by core/sheath melt-spinning without solvent [29], which is significantly different from the wet electro-spinning and wet polymer spinning reported. This solvent-free approach involves no microspheres, and it yields CNF with different morphology and microstructure of carbon materials from those by the wet electro-spinning approach. In a continuous effort, we proceed to investigate and compare the various chemical activation treatments on the CNF thus prepared, with particular emphasis on the qualitative description and quantitative estimation on the surface topology by AFM, and their relation to the microstructure of ACNF.

Experimental

Materials

PF (Novolac type, Dynea Singapore PTE Ltd), PE (Lotrene MG70, Qapco Ltd.), PP (Pro-fax PT231, Taiwan Polypropylene Co. Ltd.) were used as received. Hydrochloric acid (HCl, 36.5%) was supplied by Riedel-de Haen AG. Formaldehyde solution (HCHO, extra pure grade) was supplied by Union Chemical Works Ltd. H_3PO_4 (85%, Nihon Shiyaku Reagent) and KOH (85%, Riedel-de Haen AG) were used as received.

Preparation of ACNF

The core sheath fiber (CSF) is a specific fiber in which the primary core component was fully and evenly covered by the second sheath component. The first stage of melt-spinning was performed with the aid of two single-screw extruders joined to a spinneret containing 48 orifices. The extruders were set with five different temperature zones ranging from 150 to 220 °C along the extruder barrel. The PP resin was extruded into the core part and the PF/PE mixture was extruded into the sheath part through the spinneret. In the second stage, the CSF after melt-spinning was stabilized in a solution containing HCl (12 wt%) and HCHO (18 wt%); it was later neutralized with aqueous ammonia, washed with water, and dried at 80 °C for 1 h to form carbon fiber precursor (CFP). It was finally extracted by acetone for 24 h, washed with water, and then dried at 80 °C for 1 h. Crosslinking reaction between the linear PF chains took place during this stabilization stage.

The third stage involves removal of PP and PE from the stabilized CFP by carbonization at 800 °C for 1 h (with a heating rate 5 °C/min from 30 to 800 °C) in furnace under nitrogen atmosphere, followed by various chemical activation treatments, to yield ACNF. There were three chemical activation routes designated as ACNF-1, ACNF-2, and ACNF-3. For comparison, sample without chemical activation, designated as CNF, was also prepared by direct carbonization of stabilized CFP at 800 °C for 1 h, as schematically described in Fig. 1.

Preparation of ACNF-1

Sample CNF thus prepared was subsequently chemically activated to become ACNF-1 by immersing in a potassium hydroxide solution at 80 °C for 2 h; it was then washed with water and dried at 80 °C for 1 h. The activated CNF was then heated, as in the carbonization process, at 800 °C for 1 h in furnace under nitrogen atmosphere (with a heating rate 5 °C/min from 30 to 800 °C).
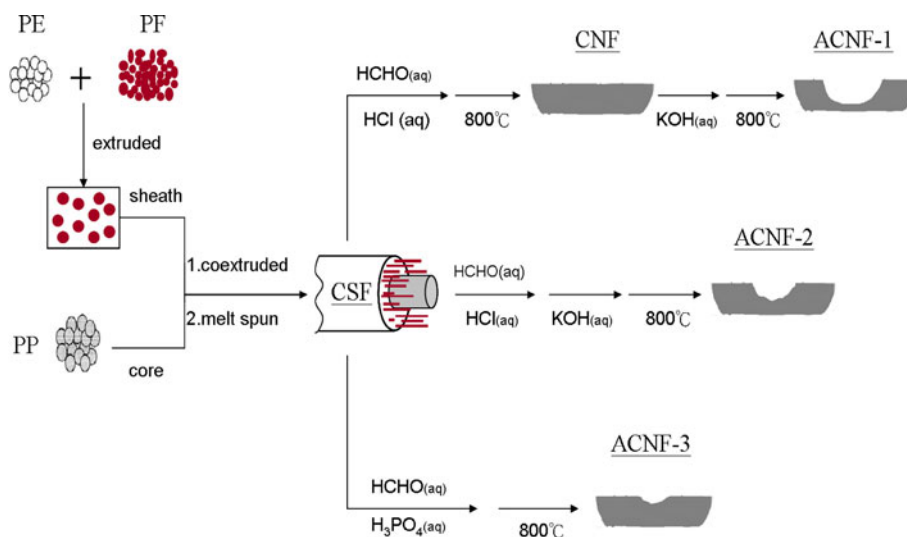
Preparation of ACNF-2

The stabilized CFP was first activated by immersing in a potassium hydroxide solution at 80 °C for 2 h; it was then washed with water and dried at 80 °C for 1 h, followed by the same carbonization process described above.

Preparation of ACNF-3

The CSF was stabilized and then activated in a solution containing phosphoric acid and formaldehyde; it was later neutralized with aqueous ammonia, washed with water, and dried at 80 °C for 1 h to form CFP. This

Fig. 1 Schematic illustrating the manufacturing process of ACNF

H_3PO_4-containing CFP was converted into ACNF-3 after simultaneous removal the PP and PE and chemical activation during the same carbonization process described above.

Characterization

Surface morphology of CNF and ACNF were examined by scanning electron microscopy (SEM, JSM-5200, JEOL^{TM}) operated at 20 kV and by AFM (NanoMan NS4+D3100, Digital Instrument) with the NanoWorld Pointprobe NCH-10 probe; With a tip radius of 8 nm, the AFM was operated in a non-contact mode on an area $\sim 140 \times 140$ nm or less. There are three important parameters which can be derived from a typical AFM measurement. Among them, RMS is the root-mean-square deviation of the mean surface values between the reference markers; R_a is the mean value of the roughness curve relative to the center line; and R_{max} is the difference in height between the highest and lowest points on the cross-sectional profile relative to the center line over the length of the profile. The crystalline phases were determined by X-ray diffractometry (XRD, D-5000, Siemens) with Cu Kα radiation (0.154 nm) and fixed slit operating at 40 kV/30 mA. Microstructure characterization and the selected area electron diffraction (SAED) ring patterns were made by analytical scanning transmission electron microscopy (AEM, JEM-3010, JEOL^{TM}) and high-resolution field emission gun transmission electron microscopy (FEG-HRTEM, Tecnai^{TM} G2 F20, FEI/Philips); the latter was operated at 200 kV. All TEM samples were ultrasonicated in ethanol and filtered on holey carbon grids prior to microscopic observations. The Raman Spectrometer used here was a Horiba Jobin-Yvon T64000 instrument for microstructure analysis. Samples for Raman were excited under a 532 nm laser source at 10 mW and under ambient conditions. The scattered light was collected in the back scattering

configuration. The analyzed region was directly visualized through an $100\times$ microscope objective. The spectra were recorded at a 0.8 cm^{-1} resolution and averaged over three scans to improve the signal-to-noise ratio.

Results and discussion

Surface morphology

Morphology by scanning electron microscopy

SEM images of CNF and ACNF samples in Fig. 2 all show long and winding fibers having diameter of 100–600 nm, with an average diameter ~ 400 nm and length greater than 80 μm. In general, rather smooth and clean surfaces with constant diameter for each fiber are present for all the fibers prepared in this work. Fibers of the HCl-stabilized and KOH-activated ACNF-1, and ACNF-2 tend to be regularly oriented into bundles and the bundles appear rather compliant and curl up to become rolls of wavy long ones, whereas the bundles of phosphoric acid-stabilized-and-activated ACNF-3 seem relatively straight and rigid.

A closer look under higher magnifications on a single fiber in Fig. 3 reveals several irregular cavities having 5–50 nm in diameter on the fiber surface of ACNF-1; these cavities result from the KOH-etched CNF surfaces which were carbonized twice [5]. On the other hand, worm-like grooves with ~ 7 nm in width are evenly distributed all over the surface of ACNF-2; these grooves may result from the uncured PF polymer chains which were dissolved by KOH during the CFP stage. In addition, surface of CNF and ACNF-3 seem relatively smooth and clean, with only subnanoscale roughness not discernible under SEM. Table 1 summarizes the SEM observations for comparison.
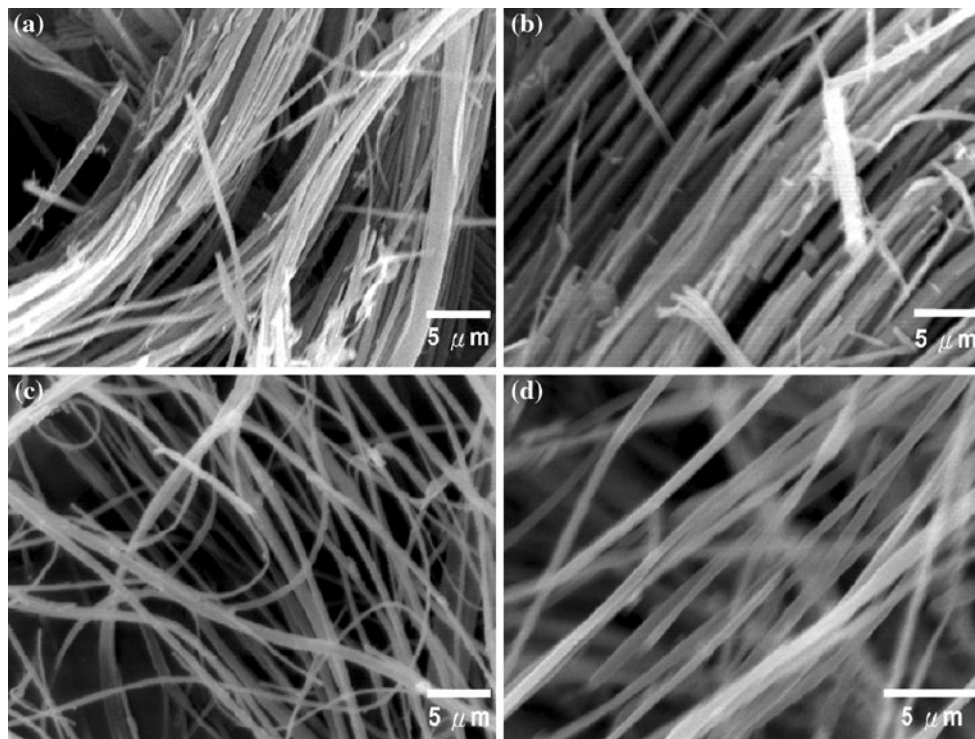
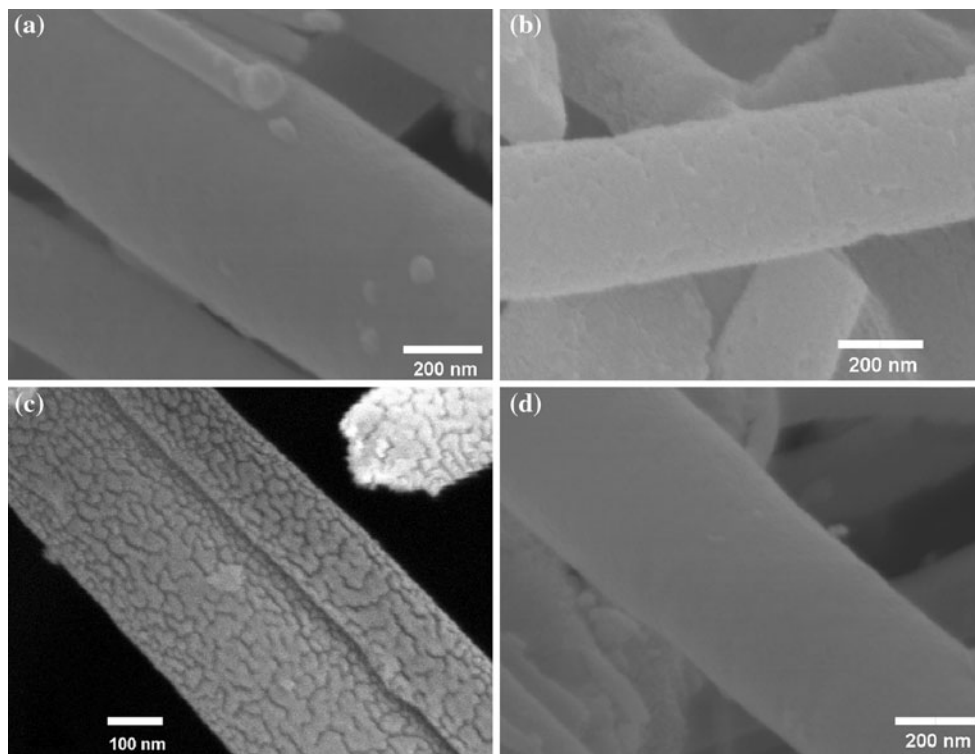**Fig. 2** SEM images showing surfaces of **a** CNF, **b** ACNF-1, **c** ACNF-2, **d** ACNF-3
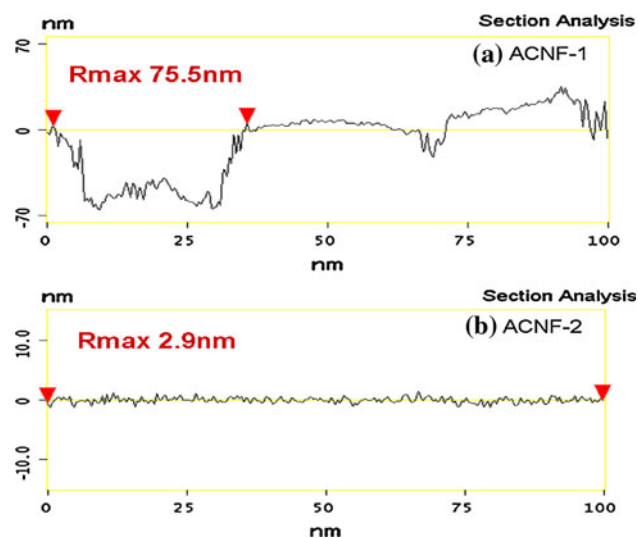

Fig. 3 SEM images under high magnification showing surfaces of **a** CNF, **b** ACNF-1, **c** ACNF-2, **d** ACNF-3

Table 1 Surface morphology and fiber diameter of CNF and ACNFs by SEM

Sample	Fiber diameter (nm)	Morphology
CNF	378 ± 93	Evenly spread nanopores
ACNF-1	401 ± 131	Irregular cavities 5–50 nm in dia.
ACNF-2	378 ± 128	Worm-like grooves ∼7 nm width
ACNF-3	434 ± 107	Evenly spread nanopores

Fig. 4 AFM section analysis of **a** ACNF-1 and **b** ACNF-2

Topography by atomic force microscopy

Sectional analysis from AFM provides a more direct and concise appraisal on surface roughness. This is depicted in Fig. 4 where a particular section of sample surface was selected. An irregular cavity with ∼34 nm in width and maximum height $R_{max} = 75.5$ nm in depth is identified for ACNF-1, indicating a rather rough surface. This observation is quite consistent with the SEM results. For comparison, sample ACNF-2 with a less rough surface has a value of $R_{max} = 2.9$ nm. Shown in Fig. 5 are the three-dimensional images from AFM measurements where the sample surfaces were scanned line-by-line. The highly sharp contrast and large dark area of sample ACNF-1 suggest deep and wide cavities, and thus a high surface roughness. All the other three images in Fig. 5 display lesser rough surface than that of ACNF-1 [14, 23, 30].

Surface roughness can better be quantified by certain statistically meaningful parameters such as the maximum height (R_{max}), mean roughness (R_a), and root-mean-square (RMS); these parameters are compared among the activated and non-activated CNFs in Table 2 [31, 32]. Each individual result is an average value of three measurements

at randomly chosen locations. The value of R_{max} increases from 4.3 (CNF) to 26.3 nm (ACNF-1), R_a from 0.6 to 5.4 nm, and RMS from 0.8 to 13.9 nm; whereas the also activated samples ACNF-2 and ACNF-3 do not show much improvement over the unactivated CNF.

Microstructure analysis

Raman scattering

Raman profiles of CNF and ACNFs are shown in Fig. 6. The spectra, characterized by two peaks near 1343 and 1597 cm^{-1}, are typical in the high wave-number region of CNFs. The peak at 1343 cm^{-1} is due to the disordered portion of the carbons (D-band) since it is absent in highly oriented pyrolytic graphite. The peak near 1597 cm^{-1} is indicative of the ordered graphitic crystallites of the carbons (G-band) [33], since it is near the G-peak for the typical graphitic carbons normally found at 1580 cm^{-1}. In particular, sample ACNF-1 shows strong graphitic nature as its G-band can further be resolved into two discernible peaks, with a sharp peak at 1578 cm^{-1} and a shoulder at 1615 cm^{-1}; the latter peak is near the disordered carbon structure at 1620 cm^{-1} (so-called D′-peak) [34, 35]. Thus, sample ACNF-1 may have the graphitic particles embedded homogeneously in an amorphous carbon phase.

The degree of crystallinity can also be quantified by the intensity ratio I_D/I_G from Raman spectra [36], where I_D and I_G are the integrated intensity of the D- and G-band, respectively. Results from Table 3 indicate that activation treatment on CNF generally promotes the crystalline formation as I_D/I_G increases from 1.34 for CNF to as high as 0.92 for ACNF-1. Yet, values of ACNFs are still much higher than that of the crystalline graphite ($I_D/I_G = 0.1$–0.3), implying a lower degree of crystallinity.

Selected area electron diffraction

SAED ring patterns of CNF and ACNFs on a single nanofiber are shown in Fig. 7; in general, three thin diffraction rings around the center spot can be identified. These suggest that there exist both an ordered phase and a disordered phase in samples CNF and ACNFs; note that similar result about a dual-phase of CNF has been reported [37, 38]. For ACNF-1, a discernible pairs of small arcs for (002) plane and a weak ring for (100) plane can be identified from Fig. 7, suggesting a graphitic orientation of (002) planes. For samples ACNF-2 and CNF, no clear arc but ring patterns for (002) and (100) are identified, suggesting a less graphitic order with some mixed amorphous phase. Sample ACNF-3 displays only halos without any arc or ring, implying a most amorphous microstructure in nature.

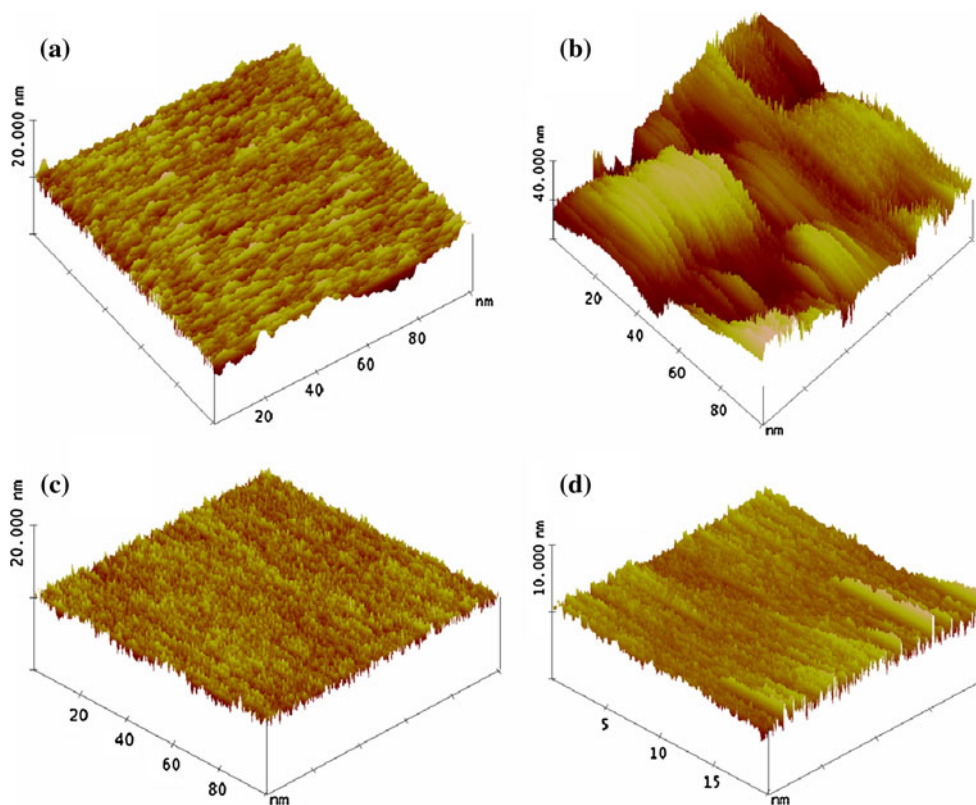**Fig. 5** Three-dimensional AFM images (100 × 100 nm) of **a** CNF, **b** ACNF-1, **c** ACNF-2, **d** ACNF-3

Table 2 Surface characteristics of CNF and ACNFs by AFM

Sample	R_{max} (nm)	R_a (nm)	RMS (nm)
CNF	4.3 ± 0.8	0.6 ± 0.1	0.8 ± 0.1
ACNF-1	26.3 ± 13.2	5.4 ± 2.1	13.9 ± 3.4
ACNF-2	2.7 ± 0.4	0.4 ± 0.0	0.5 ± 0.1
ACNF-3	2.5 ± 0.6	0.3 ± 0.1	0.9 ± 0.5

Table 3 Summary on microstructure of CNF and ACNFs

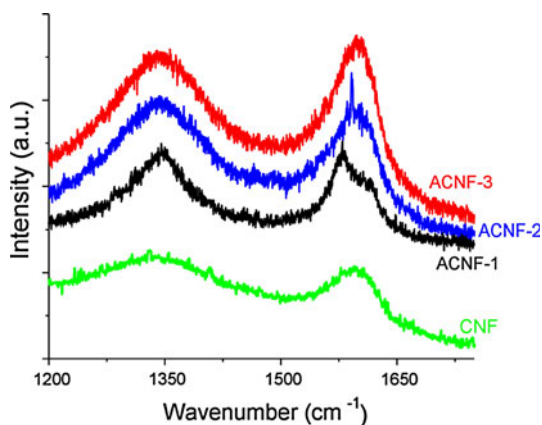| Sample	Raman I_D/I_G	SAED	XRD d_{002} (nm)
CNF	1.34	Ring patterns for (002), (100)	0.355
ACNF-1	0.92	Pairs of arc for (002), (100)	0.344
ACNF-2	1.18	Ring patterns for (002), (100)	0.359
ACNF-3	1.12	Halos	0.385

Fig. 6 Raman spectra of CNF and ACNFs

X-ray diffractometry

The wide-angle XRD profiles of CNF and ACNFs in Fig. 8 show two discernible diffraction peaks. The peak at low diffraction angles corresponding to $2\theta = 23°–26°$ is assigned to the graphitic (002) plane; whereas the peaks located near $2\theta = 41°–43°$ is assigned to the (100) plane. Sample ACNF-1 displayed the graphitic carbon structure with a sharp (002) peak at $2\theta = \sim25.9°$, accompanied by a small yet discernible (100) peak. The interlayer distance between the graphene planes (d_{002}) determined from the Bragg's law is 0.344 nm, as compared to 0.355 nm for
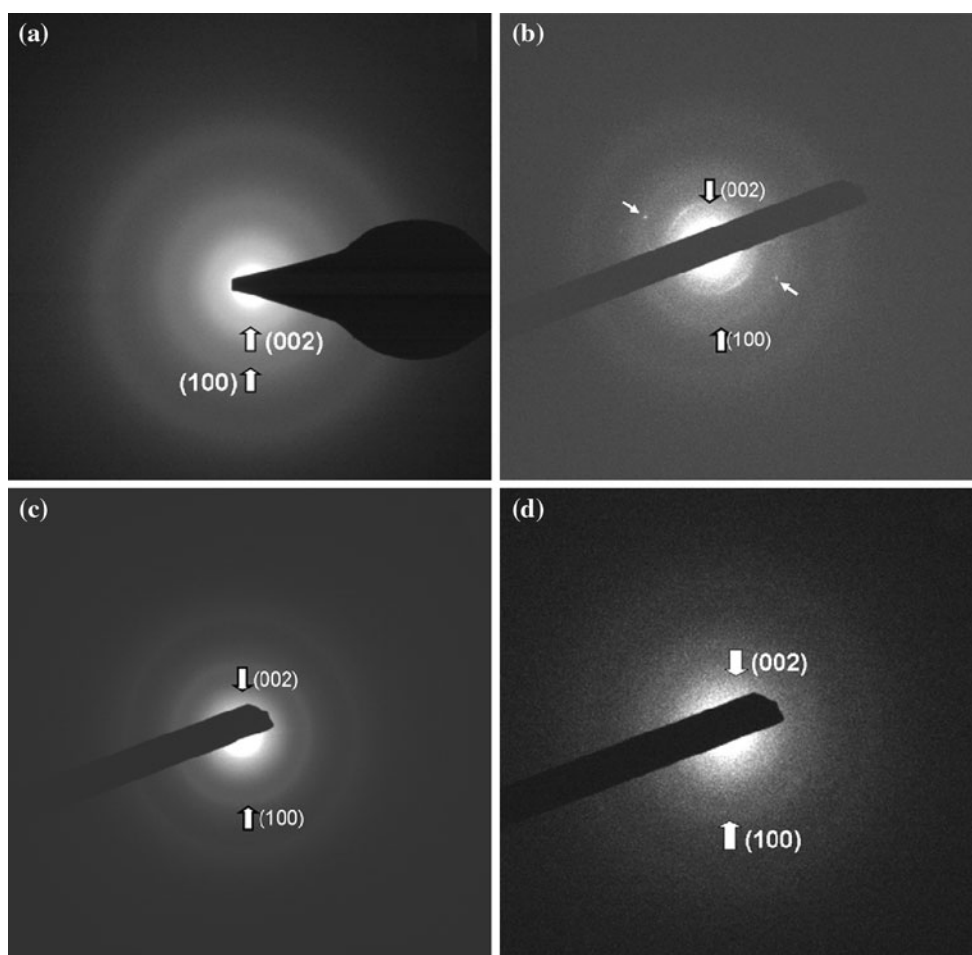
Fig. 7 SAED ring patterns of **a** CNF, **b** ACNF-1, **c** ACNF-2, **d** ACNF-3

sample CNF; both are larger than that of the ideal crystalline graphite ($d_{002} = 0.335$ nm), This again suggests a dual-phase nature of the activated CNF in this study [35]. The XRD results match very well with strong G-band in Raman spectrum (Fig. 6) and the sharp (002) arc in SAED pattern (Fig. 7). In general, higher crystallinity (with more graphitic component) can be found for activated samples ACNF-1 than the other activated samples including (ACNF-2 and -3) and un-activated CNF, when one compares the diffraction peaks in Fig. 8 and the interlayer spacing in Table 3. Apparently, a higher carbonization temperature (as high as 3000 °C) is required in order to obtain the ordered turbostatic graphite structure and to promote the crystallinity of the activated CNF in this study [39, 40].

Evaluation of activation methods

A comparison on the activation methods provides further insight into the morphological results obtained above. For sample ACNF-1, it was the surfaces of the
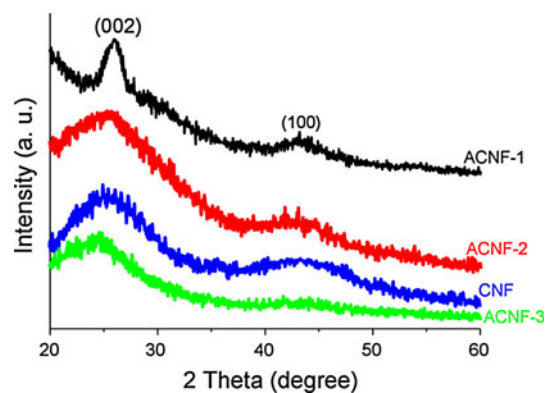

Fig. 8 XRD profiles of CNF and ACNFs

already-stabilized-and-carbonized CNF which were chemically corroded and etched by KOH, followed by a second carbonization to finally produce the ACNFs having micropores and mesopores. The activating agent KOH in this case possesses high activation efficiency when interacting with CNF. In essence, KOH preferentially attacks the amorphous portions of the carbon, resulting in the formation of cavities

on the fiber surfaces; at the same time, small molecules like CO_2 and CO were released. These cavities continue to propagate in depth due to the penetration of the molten KOH.

For samples ACNF-2 and ACNF-3, it was the surfaces of the carbon fiber precursors, not the CNF, which were chemically corroded and etched by the activating agent KOH (ACNF-2) and H_3PO_4 (ACNF-3), respectively. It was originally thought that the surfaces of carbon fiber precursors would be easier to be activated than those of CNF since mechanical strength of carbon material should not be fully developed at this stage. It was later identified that the non-curing PF polymer chains of PF precursor were soluble in KOH solution. This reduces the activation efficiency of KOH, resulting in a surface morphology with irregular worm-like micro-grooves of sample ACNF-2.

Unlike the HCl-catalyzed crosslinking of PF in samples ACNF-1 and ACNF-2, here the H_3PO_4 in preparation of sample ACNF-3 was designed to serve as a double identity which has the crosslinking effect on PF on one hand, and activation effect on the then crosslinked carbon fiber precursors on the other hand. Yet, the H_3PO_4-catalyzed PF reaction seems to be able to form a rigid crosslinked structure covering the surfaces of the carbon fiber precursors, preventing them from infiltration of phosphorous compounds and further from being chemically eroded and etched by H_3PO_4, thus resulting in the nanoscaled roughness surfaces of ACNF-3.

Conclusions

We have demonstrated in this study the preparation and microscopic characterization of a series of activated amorphous CNFs by a novel solvent-free coextrusion and melt-spinning of polypropylene/(phenol formaldehyde-polyethylene)-based core/sheath polymer blends. Several irregular cavities having 5–50 nm in diameter appear on the fiber surface of the KOH-activated ACNF in which the CNF was activated; whereas worm-like grooves with ∼7 nm in width are evenly distributed all over surface of ACNF in which the CFP was activated. On the other hand, relatively smooth and clean surface of the phosphoric acid-stabilized and activated ACNF is identified, with only subnanoscale roughness.

Results from AFM reveal that the value of R_{max} increases from 4.3 nm for the un-activated CNF to 26.3 nm for the KOH-activated ACNF, R_a from 0.6 to 5.4 nm, and RMS from 0.8 to 13.9 nm. Results from XRD, Raman spectroscopy, and SAED indicate the KOH-activated ACNF is a mixed-phase carbon material consisting of a crystalline graphitic particles embedded homogeneously in an amorphous carbon matrix; whereas the phosphoric acid-activated ACNF tends to be a disordered random carbon phase. The

activating agent KOH is found to be highly efficient when interacting with CNF, preferentially attacking the amorphous portions of the carbon, resulting in the formation of cavities on the fiber surfaces; these cavities continue to propagate in depth due to the penetration of the molten KOH.

References

1. Kim YJ, Horie Y, Matsuzawa Y, Ozaki S, Endo M, Dresselhaus MS (2004) Carbon 42:2423
2. Barranco V, Lillo-Rodenas MA, Linares-Solano A, Oya A, Pico F, Ibanez J et al (2010) J Phys Chem C 114:10302
3. Endo M, Kim YJ, Fujino T, Oyama S, Naohiko O, Sato K et al (2002) Mol Cryst Liq Cryst 388:481/67
4. Endo M, Kim YJ, Nishimura Y, Inoue T, Ohta H, Dresselhaus MS et al (2002) Carbon 40:2613
5. Kim YJ, Kim YA, Chino T, Suezaki H, Endo M, Dresselhaus MS (2006) Small 2:339
6. Jiang Q, Qu MZ, Zhou GM, Zhang BL, Yu ZL (2002) Mater Lett 57:988
7. Blackman JM, Patrick JW, Arenillas A, Shi W, Snape CE (2006) Carbon 44:1376
8. Suarez-Garcia F, Vilaplana-Ortego E, Kunowsky M, Kimura M, Oya A, Linares-Solano A (2009) Int J Hydrogen Energy 34:9141
9. Jimenez V, Sanchez P, Diaz JA, Valverde JL, Romero A (2010) Chem Phys Lett 485:152
10. Zubizarreta L, Arenillas A, Pis JJ (2009) Int J Hydrogen Energy 34:4575
11. Im JS, Park SJ, Lee YS (2009) Mater Res Bull 44:1871
12. Bui NN, Kim BH, Yang KS, Dela Cruz ME, Ferraris JP (2009) Carbon 47:2538
13. Ra EJ, Raymundo-Pinero E, Lee YH, Beguin F (2009) Carbon 47:2984
14. Paredes JI, Martinez-Alonso A, Tascon JMD (2006) Langmuir 22:9730
15. Macia-Agullo JA, Moore BC, Cazorla-Amoros D, Linares-Solano A (2004) Carbon 42:1367
16. Kim BJ, Lee YS, Park SJ (2007) J Colloid Interface Sci 306:454
17. Luxembourg D, Py X, Didion A, Gadiou R, Vix-Guterl C, Flamant G (2007) Microporous Mesoporous Mater 98:123
18. Perrin A, Celzard A, Albiniak A, Kaczmarczyk J, Mareche JF, Furdin G (2004) Carbon 42:2855
19. Yue Z, Economy J, Mangun CL (2003) Carbon 41:1809
20. Barranco V, Lillo-Rodenas MA, Linares-Solano A, Oya A, Pico F, Ibanez J et al (2009) Electrochim Acta 54:7452
21. Kashiwase Y, Ikeda T, Oya T, Ogino T (2008) Appl Surf Sci 254:7897
22. Hoffman WP (1992) Carbon 30:315
23. Paredes JI, Martinez-Alonso A, Tascon JMD (2000) Carbon 38:1183
24. Paredes JI, Martinez-Alonso A, Tascon JMD (2001) Carbon 39:1575
25. Kim YA, Matusita T, Hayashi T, Endo M, Dresselhaus MS (2001) Carbon 39:1747
26. Paredes JI, Burghard M, Martinez-Alonso A, Tascon JMD (2005) Appl Phys A 80:675
27. Figueiredo JL, Serp PH, Nysten B, Issi JP (1999) Carbon 37:1809
28. Bellucci S, Gaggiotti G, Marchetti M, Micciulla F, Mucciato R, Regi M (2007) J Phys Conf Ser 61:99

29. Cheng K-K, Hsu T-C, Kao L-H (2011) J Mater Sci 46:1870. doi:10.1007/s10853-010-5015-1

30. Paredes JI, Martinez-Alonso A, Tascon JMD (2003) Microporous Mesoporous Mater 65:93

31. Hirose M, Ito H, Kamiyama Y (1996) J Membr Sci 121:209

32. Zhu XD, Ding F, Naramoto H, Narumi K (2006) Appl Surf Sci 253:1480

33. Endo M, Kim C, Karaki T, Kasai T, Matthews MJ, Dresselhaus MS et al (1998) Carbon 36:1633

34. Beyssac O, Goffe B, Petitet JP, Froigneux E, Moreau M, Rouzaud JN (2003) Spectrochim Acta A 59:2267

35. Yang KS, Kim C, Park SH, Cho JI, Lee DY, Lee WJ et al (2004) J Raman Spectrosc 35:928

36. Ermolieff A, Chabli A, Pierre F, Rolland G, Rouchon D, Vannuffel C et al (2001) Surf Interface Anal 31:185

37. Kishore N, Sachan S, Rai KN, Kumar A (2003) Carbon 41:2961

38. Salver-Disma F, Tarascon JM, Clinard C, Rouzaud JN (1999) Carbon 37:1941

39. Kasahara N, Shiraishi S, Oya A (2002) Carbon 41:1654

40. Sharma A, Kyotani T, Tomita A (2000) Carbon 38:1977